Analytical and Bioanalytical Chemistry (2020) 412:7321–7332
https://doi.org/10.1007/s00216-020-02866-4

RESEARCH PAPER

Preparation, characterization, and application of soluble liquid crystalline molecularly imprinted polymer in electrochemical sensor

Li-Ping Zhang[1] · Ze-Hui Wei[2] · Su-Na He[1] · Yan-Ping Huang[2] · Zhao-Sheng Liu[2]

Received: 4 June 2020 / Revised: 27 July 2020 / Accepted: 5 August 2020 / Published online: 12 August 2020

Abstract

A novel soluble molecularly imprinted polymer (SMIP) without chemical cross-linker was successfully synthesized. The quinine (QN), which the structure was similar to the template, was chosen as the immobile template to improve the affinity of MIP. 4-Methyl phenyl dicyclohexyl ethylene (MPDE) was used as the liquid crystal (LC) monomer to increase the rigid of the composite. The cooperative effect of QN and MPDE was demonstrated by comparing with the conventional MIP, which synthesized without QN and MPDE. The polymerization conditions of SMIP including the ratio of MAA to MPDE, template to functional monomer, and HQN to QN were also optimized. Moreover, the characterizations of the SMIP were investigated by the transmission electron microscopy (TEM), field emission scanning electron microscopy (SEM), thermogravimetric analysis (TGA), X-ray diffraction (XRD), and nitrogen adsorption. In binding behavior, the SMIP presented the maximum adsorption capacity (0.37 ± 0.06 mmol/g) and imprinting factor (3.44 ± 0.25). And above all, the obtained polymer exhibited the solubility in the organic solution. In addition, the proposed SMIP as the electrochemical sensor exhibited a significant conductivity and sensitivity with the detection limit of 0.33 μM for HQN, the recoveries for the sample analysis varied from 97.4 to 100.8%, and the intra-day precision and inter-day precision were within 5.5% and 12.5%, respectively. It turned out that the SMIP had demonstrated more excellent potential than the traditional insoluble MIP in the development of the membrane-based electrochemical sensors.

Keywords Soluble molecular imprinted polymer · Immobile template · Liquid crystal monomer · Recognition performance

Introduction

Molecular imprinting is an emerging technology that could prepare the polymer with better specific recognition performance for template molecule [1], and the resultant composite was called molecularly imprinted polymer (MIP), which was prepared by polymerization with the initiator in the presence of template molecule, functional monomer, and cross-linking agent. After removing the template molecule with appropriate methods, the obtained MIP would possess imprinted sites complementary to the template. Therefore, the imprinted sites in MIP were formed by the copolymerization between cross-linker and functional monomer around the template-functional monomer complex during the polymerization process. Since the low-cost preparation, high selectivity, and reusability, the MIP had been widely applied in many fields, including solid-phase extraction [2], chromatographic separation [3, 4], drug delivery systems [5, 6], and chemical sensors [7, 8]. As the chemical sensors, the MIP could not only detect the trace pollutants in the environment and food but also the markers of the disease and tumor [9–12]. Moreover, compared with the conventional measuring methods, the MIP sensors was more sensitive, stable,

Electronic supplementary material The online version of this article (https://doi.org/10.1007/s00216-020-02866-4) contains supplementary material, which is available to authorized users.

✉ Yan-Ping Huang
huangyp100@163.com

✉ Zhao-Sheng Liu
zhaoshengliu@sohu.com

[1] School of Basic Medical Sciences, Henan University of Science and Technology, Luoyang 471000, Henan, China

[2] Tianjin Key Laboratory on Technologies Enabling Development of Clinical Therapeutics and Diagnostics (Theranostics), School of Pharmacy, Tianjin Medical University, Tianjin 300070, China

convenient, and fast. However, the rigid and highly cross-linked structures of MIP made it difficult to dissolve in the plasticized polymeric membranes, causing the less binding sites and lower sensitivity [13]. Preparing the MIP with low cross-linking that could be dissolved or easily dispersed in the medium was very imperative.

In recent years, the preparation and applications of MIP were very widespread, yet there were only a few studies on the soluble MIP (SMIP). For instance, a dendrimer by monomolecular imprinted with porphyrin as templates was demonstrated by Zimmerman et al., which exhibited the solubility in common organic solvents [14]. However, this method required intricate synthesis process. Wulff groups had prepared a type of soluble single-molecule imprinted nanogel as the enzyme catalysis by the dilution method, while the rigidity and catalytic activities were weaker than that of insoluble imprinted polymers [15]. Nowadays, Qin groups had developed novel SMIP and soluble molecularly imprinted nanorods. And the soluble MIP had been successfully applied in potentiometric sensor for detection of bisphenol AF [16, 17]. Whereas the synthesis conditions of them were relatively harsh and complex. Here, a simple method for the synthesis of the SMIP with the simple bulk polymerization utilizes liquid crystal (LC) and immobile template, quinine (QN), as the combination monomer would be described.

The LC was an intermediate state between the liquid and solid phases, presenting a rod-like structure which is rigid and flexible [18]. Among them, the mesogenic unit of the rigid part played a significant role in strengthening the polymer skeleton, and the unsaturated bond at the flexible end could participate in the polymerization [19, 20]. The liquid crystalline MIP (LC MIP) was a new type of robust MIP with LC as the auxiliary monomer. Above all, this system could decrease the cross-linking level of MIP with the substitution of partial chemical cross-linking in the process of synthesis, which alleviated the embedding problem of imprinted cavities significantly and accelerated the elution of template in polymer [21–23]. Due to easy accessibility to the imprinted sites, the obtained LC MIP exhibited much higher adsorption capacity than conventional MIP and had been successfully applied in the stationary phase for HPLC [20], CEC separation [21, 22], drug delivery [23], and biosensors [24].

The immobile templates were a class of materials with similar structure to template molecules and owned the alkene bonds at the terminal. Resembling to LC monomer, the terminal alkene bond of them could take part in polymerization to maintain the binding sites presented in polymer structures [25]. At the same time, part of them may also serve as a physical cross-linker to stabilize the polymer chain. Garcinuño et al. had synthesized a series of polymers with cross-linking levels ranging from 12 to 80%, which proved that the presence of immobile template in low cross-linked imprinted polymers had presented a positive effect on molecular recognition [26].

The hydroquinine (HQN) was a derivative of QN, which could be extracted from the cinchona barks [27]. The QN and HQN displayed better therapeutic effect on the malaria, analgesia, and muscle cramps [28, 29]. However, high dose intake of them could also cause some serious side effects, including nausea, abdominal pain, blurred vision, headache, and kidney failure [30]. The content of QN and HQN in different samples was usually detected by the HPLC, capillary zone electrophoresis, UV resonance Raman micro-spectroscopy, and other methods [31–34]. However, these methods presented the disadvantage of high cost and complex sample pretreatment process. In contrast, the electrochemical analysis was a relatively simple and rapid detection method.

In this study, the soluble MIP without a chemical cross-linker based on bulk polymerization was proposed by introducing the LC monomer and immobile template. Thereinto, the LC monomer that owned the rigid mesogenic unit and unsaturated bond at the flexible end acted as the cross-linker to participate in the polymerization. And the immobile template (QN) could also take part in the polymerization to maintain the imprinting sites of the polymer. The imprinted cavities of the SMIP were formed by the joint action of HQN, MAA, and LC monomer and QN. By optimizing the synthesis condition, the resultant SMIP showed better imprinting performance and selectivity for HQN. Besides, they also offered remarkably improved sensitivity for electrochemical detection as the sensor and could measure the trace amount of HQN in lake water successfully.

Experimental

Materials

Hydroquinine (HQN, 98.0%), quinine (QN, 99.0%), hydroquinidine (HQND, 99.0%), quinidine (QND, 99.0%), and 2-azobisisobutyronitrile (AIBN) were purchased from J&K Scientific Co., Ltd. (Beijing, China). Ethylene glycol dimethacrylate (EDMA, 98.0%) was from Sigma-Aldrich (St. Louis, MO, USA). Methacrylic acid (MAA, AR grade) was obtained from Kermel Chemical Reagent Co., Ltd. (Tianjin, China). 4-Methyl phenyl dicyclohexyl ethylene (MPDE, 99.5%) was supplied by Hebei Meixing Chemical Co., Ltd. (Hebei, China). Toluene (Tol, AR grade) was purchased from Biaoshiqi Science and Technology Development Co., Ltd. (Tianjin, China). Acetonitrile (ACN, HPLC grade) was from Concord Technology Co., Ltd. (Tianjin, China). The other reagents were supplied by Jiangtian Chemical Reagent Co., Ltd. (Tianjin, China).

Table 1 The synthesis protocol of SMIP

Polymer	HQN (mmol)	QN (mmol)	MAA (mmol)	MPDE (mmol)	EDMA (mmol)	Tol (μL)	ACN (μL)	AIBN (mg)	Q_{max} (mmol/g)	IF
1	0.1	0.1	1.6	1.4	–	900	600	18	0.206 ± 0.038	2.054 ± 0.275
2	0.1	0.1	1.6	1.6	–	900	600	18	0.325 ± 0.051	2.058 ± 0.442
3	0.1	0.1	1.6	1.8	–	900	600	18	0.265 ± 0.034	2.334 ± 0.454
4	0.1	0.1	1.6	2.4	–	900	600	18	0.213 ± 0.059	1.458 ± 0.364
5	0.1	0.1	1.6	3.0	–	900	600	18	0.149 ± 0.030	1.481 ± 0.230
6	0.1	0.1	1.6	3.6	–	900	600	18	0.195 ± 0.030	1.194 ± 0.149
7	0.40	0.1	1.6	1.8	–	900	600	18	0.142 ± 0.022	1.225 ± 0.091
8	0.20	0.1	1.6	1.8	–	900	600	18	0.210 ± 0.039	1.799 ± 0.110
9	0.16	0.1	1.6	1.8	–	900	600	18	0.372 ± 0.058	3.439 ± 0.251
10	0.08	0.1	1.6	1.8	–	900	600	18	0.213 ± 0.024	1.832 ± 0.095
11	0.05	0.1	1.6	1.8	–	900	600	18	0.235 ± 0.039	2.018 ± 0.312
12	0.16	0.04	1.6	1.8	–	900	600	18	0.280 ± 0.051	2.773 ± 0.978
13	0.16	0.08	1.6	1.8	–	900	600	18	0.256 ± 0.018	3.112 ± 0.203
14	0.16	0.12	1.6	1.8	–	900	600	18	0.284 ± 0.035	1.394 ± 0.271
15	0.16	0.2	1.6	1.8	–	900	600	18	0.303 ± 0.041	1.116 ± 0.013
CM1	0.16	0.1	1.6	–	1.8	900	600	18	0.353 ± 0.038	1.191 ± 0.049
CM2	0.16	–	1.6	1.8	–	900	600	18	0.099 ± 0.016	1.184 ± 0.253
CM3	0.16	–	1.6	–	1.8	900	600	18	0.346 ± 0.024	1.375 ± 0.141
CM4	0.16	–	1.6	–	–	900	600	18	–	–

The preparation of SMIP

The SMIP was prepared as illustrated in Table 1. The template HQN, immobilized template QN, functional monomer MAA, initiator AIBN, and the LC monomer MPDE were dissolved with Tol and ACN in a 20-mL flask. The mixture was blended further by ultrasonic cleaner for 10 min, then purged with N_2 for 10 min. Finally, the pre-polymerization solution was placed in a water bath at 60 °C for 24 h. Since the solubility in methanol and acetonitrile, the acetonitrile/water (5/5, v/v) was served as the eluant of resulted particles that were collected in a centrifugation tube. By adding 4 mL of acetonitrile/water (5/5, v/v) into them repeatedly, the HQN embedded in the polymer was sufficiently dissolved by ultrasonic cleaning machine and the content of HQN in the supernatant after centrifugation was determined by UV-vis at 238 nm. The HQN's successful removal could be confirmed until the absorbance was lower than 0.01. The obtained polymer was dried at room temperature and the schematic plot was illustrated in Fig. 1. The non-imprinted SNIP, LC-free QN MIP, and QN-free LC MIP were prepared in the same way except without template, LC monomer (replaced by EDMA), and QN, respectively. Also, the conventional MIP was synthesized as above, neither LC monomer nor QN; meanwhile, the cross-linker was replaced by EDMA.

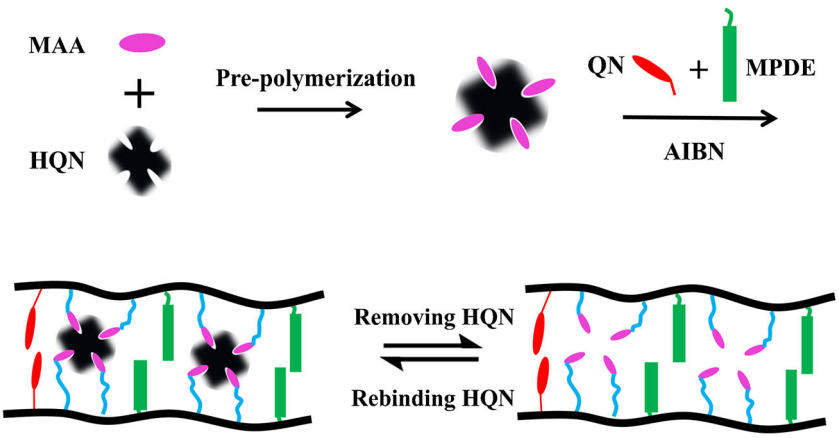

Fig. 1 Schematic illustration for the synthesis of SMIP

Characterization of SMIP

The morphologies of the SMIP, SNIP, as well as the control particle, LC-free QN MIP, QN-free LC MIP, and conventional MIP were characterized by scanning electron microscopy (SEM) (FEI Nova NanoSEM 450, Netherlands) and transmission electron microscopy (TEM) (HT-7700, Hitachi, Japan). The crystal structures of polymers were detected by X-ray diffractometer (X'Pert Pro, PANalytical, Netherlands). The thermal stability of polymers was recorded on the simultaneous thermal analyzer (TG290F3, Netzsch, Germany) at a heating rate of 20 °C/min from room temperature to 600 °C under N_2. The nitrogen adsorption-desorption experiments were measured by a pore size distribution analyzer (V-Sorb 2800TP, Gold APP Instruments Corporation China, Beijing, China).

Selection of dispersion medium

In order to select the best dispersion medium, several copies of 10 mg dried SMIP were placed in 5-mL centrifuge tubes. Then, 3 mL of different dispersion medium, including acetonitrile, methanol, ethanol, distilled water, dimethyl sulfoxide, acetonitrile/water (6/4, v/v), acetonitrile/water (5/5, v/v), and acetonitrile/water (3/7, v/v), were added into them separately. After shaken for 5 h on the constant temperature oscillator, the mixtures were centrifuged at 10,000 rpm for 10 min. Finally, the remaining precipitate was dried and weighed.

Binding properties of SMIP

The binding capacity of HQN on SMIP was achieved by equilibrium adsorption experiment. 2.0 mL of HQN solution (0~2.5 mmol/L) prepared by acetonitrile/water (5/5, v/v) solvent was put into the dried composite weighted 10 mg. After shaken for 5 h and centrifuged, the concentration of HQN in the supernatant was determined by UV spectrophotometer at the wavelength of 238 nm. The adsorption kinetic experiment was similar to the above description, except for that it needs to test samples at different time points. The above adsorption capacity (Q_e, mmol/g) of HQN on SMIP was calculated as follows: $Q_e = (C_0\text{-}C_e)\ V/M$, where C_0 and C_e (mmol/L) represented the initial and equilibrium concentration of HQN in acetonitrile/water (5/5, v/v) solution, respectively. V (L) represented the volume of the solution and M (g) was the mass of the polymer. The imprinting factor (IF) was used to evaluate the specific imprinted performance of SMIP [35]: $\mathrm{IF} = Q_{\mathrm{SMIP}}/Q_{\mathrm{SNIP}}$, where the Q_{SMIP} and Q_{SNIP} (mmol/g) represented the maximum adsorption capacity of HQN on SMIP and SNIP, respectively.

Electrochemical measurement of SMIP

The preparation of SMIP-based electrochemical sensor

The preparation processes of SMIP-based membrane were as follows: 5 mg of multi-walled carbon nanotubes (MWCNT) were dispersed in 5 mL DMF solution for standby. The chitosan solution was obtained by dissolving the chitosan (20 mg) into the 10 mL mixtures of acetonitrile/water/acetic acid (1/1/0.2). Then, the SMIP-based membrane was prepared by adding 20 mg of the SMIP into above mixtures and mixed uniformity with ultrasound oscillations. Finally, 0.5 mL of the MWCNT dispersion solution, which was mainly used to improve the conductivity of the SMIP, was added into the SMIP-based membrane and blended by sonication for 10 min [36, 37]. The glassy carbon electrodes (GCEs) were successively polished with 0.3 and 0.05 μm alumina powder, and then washed with ethanol and deionized water for 10 min, respectively. Twenty microliters of the membrane cocktail was drop-cast onto the surface of the GCEs and allowed to dry for 5 h. The obtained modified electrode was recorded as MWCNT/SMIP/GCEs.

Electrochemical measurements

The electrochemical properties of the MWCNT/SMIP-modified electrode (MWCNT/SMIP/GCE) were verified by the cyclic voltammetry (CV) and differential pulse voltammetry (DPV) using the 5 mmol/L $K_3[Fe(CN)_6]$ with 20 mmol/L KCl solution as the electrochemical probe. The amount of HQN was determined by incubating the MWCNT/SMIP/GCEs into HQN/PBS solution with different concentration for 10 min. After washing with deionized water, the modified electrode was placed in a blank PBS solution (pH 7.4, 100 mmol/L) and measured by differential pulse voltammetry (DPV). From them, the CV experiments were carried out over a potential range from − 0.2 to 0.6 V with the scan rate of 50 mV/s, and the DPV detections were characterized at the potential range from − 0.2 to 0.6 V, the potential increment was 4 mV, the pulse amplitude was 50 mV, the pulse period was 100 ms, the pulse width was 40 ms, and the sampling width was 10 ms.

Results and discussion

Solubility test

Due to the lack of chemical cross-linking agent, the stability of the MIP prepared in this work was greatly weakened. Although the immobilized template (QN) and liquid crystal monomers (MPDE) in the system could maintain the rigid

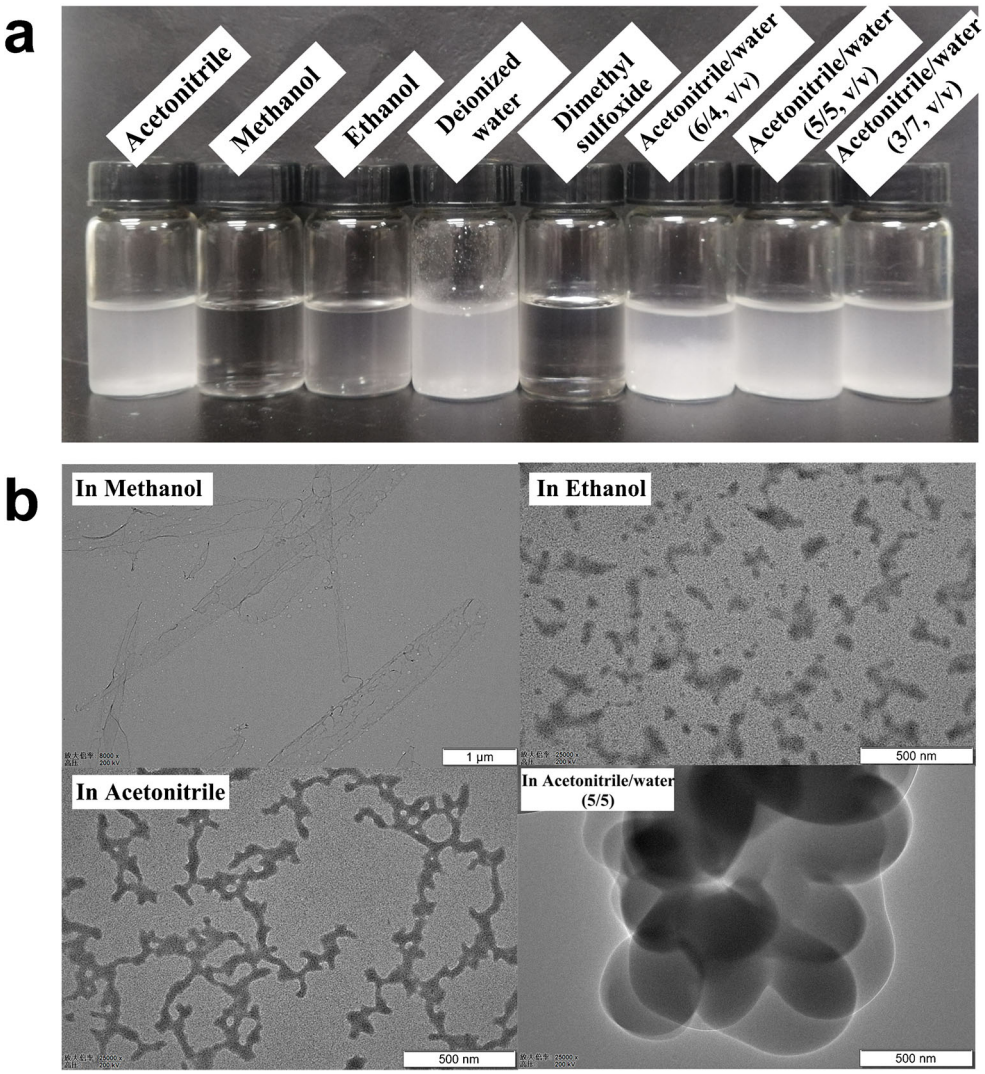

Fig. 2 Solubility (**a**) and TEM images (**b**) of SMIP in different solvents

structure of the polymer, the stability the polymer was also much lower than that of containing chemical cross-linker. Strangely, the SMIP synthesized in this system exhibited partial solubility in some organic solvents (Fig. 2a). To certify the soluble amount further, the surplus of pre-weighed MIPs (10 mg) was also recorded after shaken for 5 h in the common solvents. As shown in Table S1 (see Electronic Supplementary Material ESM), more than half of the SMIP dissolved in acetonitrile and ethanol, and almost completely in methanol. Due to its floatability [38], the SMIP in deionized water and DMSO was suspended on the surface of the medium, so as to the content of them could not be accurately measured after centrifugation. However, when the mixture of acetonitrile and water was chosen as the dispersion medium, it was found that the loss of SMIP was almost the same that in acetonitrile/water (5/5, v/v) was the least. Then, the morphologies of SMIP in the solvent were conducted further. Resembling to Fig. 2 a, the TEM image of SMIP showed no particles when using methanol as the dispersing agent, while uniform distribution in acetonitrile and ethanol, and aggregation in acetonitrile/water (5/5, v/v) (Fig. 2b). We preliminary concluded the SMIP could be soluble in methanol as molecules or ions and distributed as particle in ethanol, acetonitrile, and acetonitrile/water.

Selection of incubation medium

In order to achieve the measurement of the binding isotherm accurately, the acetonitrile/water, which the SMIP could isolate completely from them after centrifugation, was selected as the incubation solution. Firstly, the equilibrium adsorption experiments were performed in the acetonitrile/water (5/5, v/v) and acetonitrile/water (6/4, v/v) and the result was analyzed with Langmuir equation [35]: $Q_e = Q_{max}KC_e/(1 + KC_e)$, where Q_{max} (mmol/g) was the maximum amount of HQN adsorbed on SMIP, and K (L/mmol) was the constant related to the binding affinity. As illustrated in ESM Fig. S1, the SMIP demonstrated good specificity recognition performance

on HQN in both solutions, while the larger adsorption capacity (Q_{max} = 149 μmol/g) and the imprinting factor (IF = 1.786) in the acetonitrile/water (5/5, v/v) can be displayed. In conclusion, the acetonitrile/water (5/5, v/v) was casted as the best dispersion medium for the following researches.

Optimization of polymerization variables

The ratio of MAA to MPDE

In this system, the synthesis of SMIP was achieved by completely replacing the LC monomer (MPDE) with the chemical cross-linker (EDMA), expected to stabilize the rigid structure of the polymer with MPDE alone. Therefore, the content of MPDE directly affected the stability and selectivity of the SMIP. By varying the ratio of MAA to MPDE, ranging from 8/7 to 8/18, a series of SMIP were prepared and the binding performance was shown in Fig. 3 a. In general, the adsorption capacity and IF would gradually improve with the increasing of MPDE, which strengthened the rigidity of SMIP, while the higher content of MPDE (M4:8/12, M5:8/15, and M6:8/18) in the present study caused the adsorption capacity and IF value tends to decrease. The possible reason was that the increment of MPDE improved the cross-linking degree, making the imprinting sites of SMIP embedded and the specific adsorption capacity reduced. The adsorption capacity did not improve until the ratio reduced to 8/8 (M2), but the IF value was lower than 8/9 (M3), which indicated that the recognition performance of SMIP was changed as the content of MPDE. These results were inconsistent with previous studies that may be caused by the unstable structure of the SMIP [39]. As a compromise of IF value, the ratio of MAA to MPDE adopted in all subsequent protocols for preparing the SMIP was 8/9.

The ratio of template to functional monomer

The optimization of template to monomer ratio of the SMIP in this system was conducted by adjusting the amount of template (1/4–1/32) in the formula with fixing otherwise polymerization parameters. The ratio of template to functional monomer (T/M) had a significant effect on the affinity and imprinting efficiency of the MIP for the noncovalent imprinting [20]. As shown in Fig. 3 b, more or less of templates could not improve the imprinting effect of SMIP, the reasons were as follows: Since the higher content of template (M7:1/4 and M8:1/8), there were insufficient functional monomers to form specific imprinted cavities with template, resulting in fewer specific recognition sites and lower adsorption capacity; for another, the excess functional monomer will undergo self-polymerization as the lower content of template (M5:1/16, M10:1/20, M11:1/32), causing the reduction in the formation-effective template-monomer complex. Despite

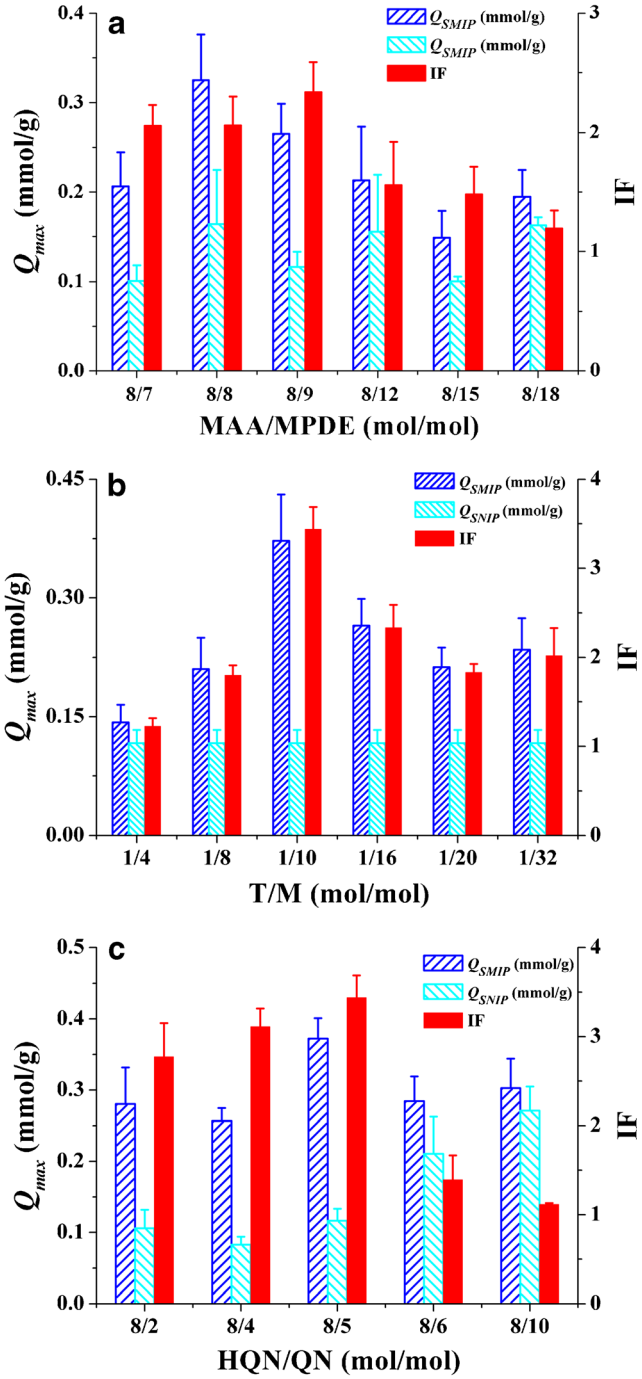

Fig. 3 Adsorption capacity and imprinting effect of HQN on SMIP prepared with different ratio of MAA to MPDE (**a**), template to functional monomer (**b**) and HQN to QN (**c**)

incompatible with the previous studies that the better imprinting effect with higher template [5, 40], the largest adsorption capacity (0.37 ± 0.06 mmol/g) and IF (3.44 ± 0.25) were achieved as the ratio of 1/10 in this system. The reason may be that the content of template showed little influence on the chain growth and condensation rate of polymerization reaction in this system that absence of chemical cross-linker.

The ratio of HQN to QN

The immobilized template, QN, in this project played an important role in the synthesis of SMIP. The double-bond structure was semblable with that of functional monomer or cross-linker, which could participate in the polymerization to stabilize the rigid structure and imprinting sites of SMIP [26]. Therefore, the influence of QN content on the imprinting effect of the SMIP was also explored. As shown in Fig. 3 c, the adsorption capacity of HQN on SNIP had improved as the content of QN increased, while the SMIP changed a little. This may be related to the higher content of immobilized template that could enhance the stability of SNIP without template and increase the non-specific adsorption for HQN, causing the IF of SMIP with HQN to QN from 8/2 to 8/5 which was relatively higher than that of 8/6 to 8/10. In addition, the other possible reasons for the reduction of SMIP adsorption capacity (8/6 and 8/10) was the embedding of few imprinting sites and the collapse of imprinting cavities in the process of grinding [41]. Therefore, by combining with the adsorption capacity (0.37 ± 0.06 mmol/g) and imprinted factor (3.44 ± 0.25) for template in Fig. 3 c, the 8/5 was confirmed as the optimal ratio of HQN to QN.

Equilibrium adsorption and selectivity of SMIP

The equilibrium adsorption performance of the HQN on the SMIP, SNIP, as well as the control composites, LC-free QN MIP, QN-free LC MIP, and the conventional MIP were investigated by the adsorption isotherm test. Due to lacking of QN, LC, or EDMA to stabilize the rigidity, the blank MIP (C4) could not be successfully synthesized. As illustrated in Fig. 4 a, the SMIP presented the greater adsorption capacity (0.37 ± 0.06 mmol/g) and imprinting effect (3.44 ± 0.25), suggesting that the cotransduction of LC monomer and immobilized template could maintain the rigid structure and improve the specific binding effect of the SMIP. While the QN-free LC MIP showed the minimal adsorption capacity compared with SMIP, which the reason was that the weaker structure was supported by MPDE only, the results demonstrated that the immobile template (QN) played an active role in stabilizing the structure of polymers. In addition, the LC-free QN MIP and conventional MIP synthesized with EDMA instead of MPDE displayed higher adsorption capacity for HQN, while the LC-free QN NIP was slightly lower than that of conventional NIP, which proved that immobilized template in the system may inhibit the generation of non-specific recognition sites of the polymer. Although with the greater binding property of conventional MIP, the imprinting effect (1.38 ± 0.14) was extremely poor, indicating that the imprinted sites of MIP with higher level of cross-linker (80–90 mol%) were embedded easily and the templates were difficult to be eluted.

The adsorption kinetics of HQN on the different MIPs was investigated in a range of the adsorption time from 0 to 300 min with a constant initial concentration. The 2 mmol/L of HQN in acetonitrile/water (5/5, v/v), which was the equilibrium concentration in adsorption isotherm (ESM Fig. S2), was adopted in this system. As shown in Fig. 4 b, the absorption amount of HQN onto SMIPs increased with the adsorption time at first 1 h, and reached equilibrium at 120 min. Similar behaviors of QN-free LC MIP were also observed with longer time for adsorption equilibrium (ca. 180 min), while the adsorption capacity was lower than that of SMIP, which may be related to the unstable structures obtained without immobile template. Strangely, the LC-free QN MIP and conventional MIP with chemical cross-linker exhibited a rapid dynamic adsorption to gain adsorption equilibrium (ca. 90 min), which suggested the recognition sites accessible for the HQN on them. Combining with the adsorption isotherm test, the specific binding effect of SMIP had been improved by introducing the LC monomer and immobilized template simultaneously, but the mass transfer of them was slower than that with chemical cross-linker.

The selectivity of SMIP was conducted by exploring the adsorption performance for the template and their analogues, the structures of the analogues were shown in Fig. 4 c. Figure 4 d demonstrated the case of SMIP and SNIP for rebinding of HQN, QN, HQND, and QND. The selectivity factor (SF) of the analogues for HQN was defined as follows: $SF = Q_M/Q_N$, where Q_M was adsorption capacity of template or its analogues on SMIP and Q_N was adsorption capacity of SNIP. The SF value of SMIP to HQN, QN, HQND, and QND was 3.44 ± 0.25, 1.17 ± 0.03, 1.11 ± 0.08, and 1.13 ± 0.02, respectively. These results manifested that the imprinted cavities of SMIP complementary to template structure could recognize the HQN specifically, while the non-specificity for QN, HQND, and QND.

Characterization of SMIP

The surface morphologies of SMIP, SNIP, and the control composites were characterized by the SEM and the results were shown in Fig. 5. The SMIP (Fig. 5a) was the cauliflower-like micro-particle of about 3 μm with an uneven surface and three-dimensional structure, the SNIP (Fig. 5b) was similar with the SMIP, but relatively loose, confirming the structural stability was inferior than that of SMIP. The LC-free QN MIP and LC-free QN NIP (Fig. 5c and d) were the bulk particles with uneven distribution, which may be caused by the combination of QN and EDMA. Since the lack of QN in the synthesis process, the QN-free LC MIP and QN-free LC NIP (Fig. 5e and f) were the irregular spherical. In addition, the conventional MIP and NIP without the QN and MPDE (Fig. 5g and h) were similar to that of LC-free QN MIP, but more dispersed, indicating that the

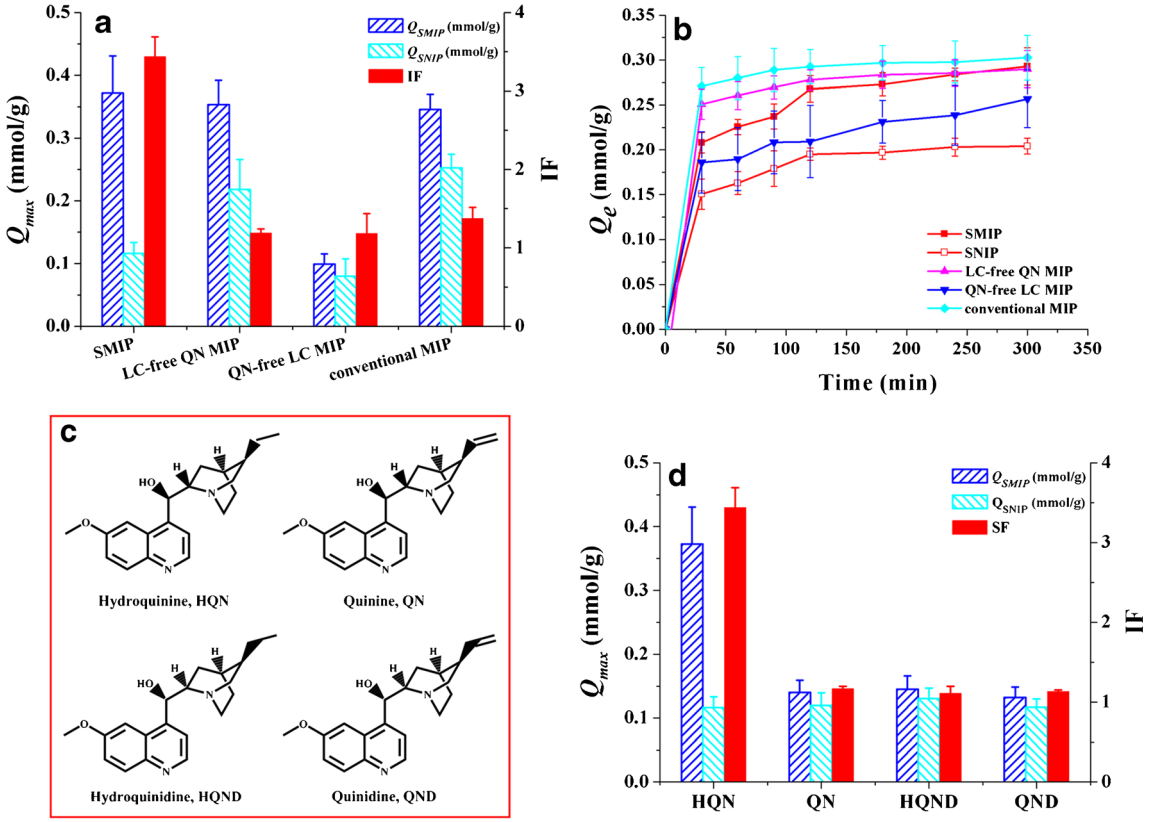

Fig. 4 **a** Imprinting effect of HQN on SMIP, LC-free QN MIP, QN-free LC MIP, and conventional MIP. **b** Kinetic binding curves of HQN on SMIP, SNIP, LC-free QN MIP, QN-free LC MIP, and conventional MIP. **c** Structure of HQN and its analogues. **d** Selectivity evaluation of HQN and its analogues on SMIP

presence of QN and MPDE exhibited prominent influence on the morphology of the SMIP.

The crystal structures of polymers were further recorded by X-ray diffraction (XRD) patterns. As shown in Fig. 6, the main characteristic peaks of LC monomer (MPDE) were observed at about 5.7°, 5.9°, 11.9°, 16.8°, 18.3°, 18.6°, 19.9°, and 20.2°. The XRD patterns of SMIP, SNIP, and QN-free LC MIP showed the good agreement with MPDE, whereas the peak intensity of them decreased significantly after synthesis. These were attributed to the amorphous structure of the MIP around MPDE that counteracting force of the MIP led to the peak strength reduction and migration [42]. The results

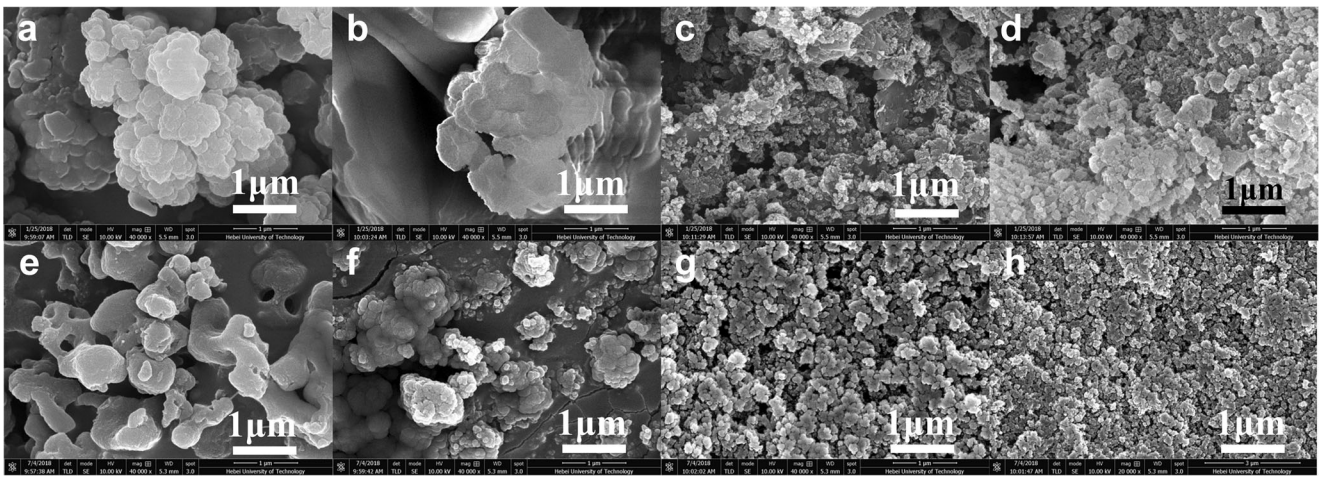

Fig. 5 SEM images of SMIP (**a**), SNIP (**b**), LC-free QN MIP (**c**), LC-free QN NIP (**d**), QN-free LC MIP (**e**), QN-free LC NIP (**f**), conventional MIP (**g**), and conventional NIP (**h**)

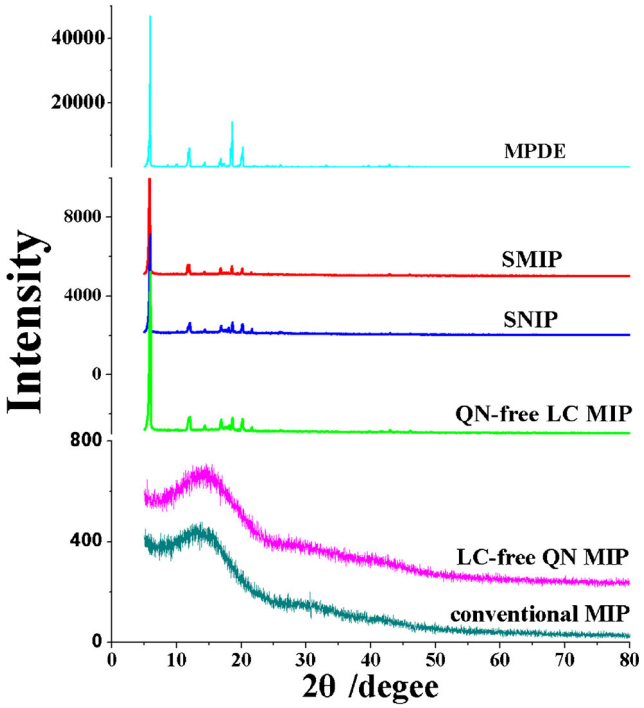

Fig. 6 XRD patterns of MPDE, SMIP, SNIP, QN-free LC MIP, LC-free QN MIP, and conventional MIP

validated the MPDE took part in the polymerization successfully. In contrast, the LC-free QN MIP and conventional MIP without MPDE demonstrated no obvious crystal peaks.

The thermal stability of the polymers at high temperature was characterized by the thermal gravimetric analysis (TGA). As shown in ESM Fig. S3, the LC-free QN MIP and conventional MIP started to decompose after 200 °C, while the SMIP, SNIP, and QN-free LC MIP were about 150 °C. Furthermore, the SMIP, SNIP, and QN-free LC MIP showed two stages of decomposition. The rapid weight loss between 150 and 260 °C was mainly caused by the collapse of the skeleton, and that in 260–450 °C, the fracture of the polymer chain was formed by the free radical of the functional monomer.

Table 2 Pore properties of SMIP, SNIP, LC-free QN MIP, QN-free LC MIP, and conventional MIP

Polymers	S_{BET} (m^2/g)	S_t (m^2/g)	V_p (cm^3/g)	D_{mean} (nm)
SMIP	5.33	5.33	0.020	14.67
SNIP	3.98	6.79	0.016	12.64
LC-free QN MIP	232.68	181.11	0.556	9.57
QN-free LC MIP	14.56	6.42	0.260	11.45
Conventional MIP	270.49	189.82	0.614	9.07

S_{BET}, BET surface area; S_t, t-plot surface area; V_P, single-point adsorption total pore volume; D_{mean}, median pore width

These results suggested that the stabilities of the SMIP and SNIP synthesized with physical cross-linker, MPDE, were not as good as that of conventional chemical cross-linker, although they presented the better specific recognition performance.

To reveal the relations between morphology and imprinting effect of MIPs, the nitrogen adsorption measurements were carried out at 77 K. As illustrated in Fig. 7 a, the SMIP, SNIP and QN-free LC MIP displayed "type III" isotherms [43] with a H3-type hysteresis loop, suggesting the pore structures of them were irregular with slit-shaped pores from aggregates of plate-like particles. On the contrary, the isotherms of LC-free QN MIP and conventional MIP with chemical cross-linker were "type II" that presented the strength interaction between the solid surface and adsorbed gas molecules. In addition, the adsorption isotherms demonstrated an inflection point at around 0.1 P/P_0, indicating the ending of the monolayer adsorption stage and the beginning of the multilayer coverage stage. Similarly, the porosity of them was also higher (Fig. 7b), and the pore diameters of the SMIP, SNIP, and QN-free LC MIP were all distributed at 4–5 nm instead of 7–8 nm or 10 nm of the LC-free QN MIP and conventional MIP. All of them were single peak, which suggested that the mesoporous polymers in this system contained a large number of slit-shaped pores and other irregular shape pores.

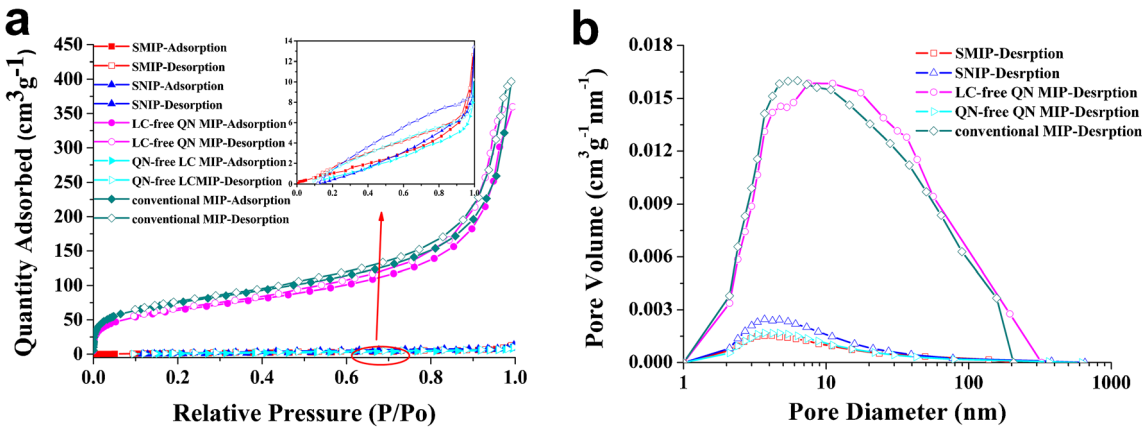

Fig. 7 Nitrogen adsorption-desorption isotherms (**a**) and pore distribution (**b**) of SMIP, SNIP, LC-free QN MIP, QN-free LC MIP, and conventional MIP

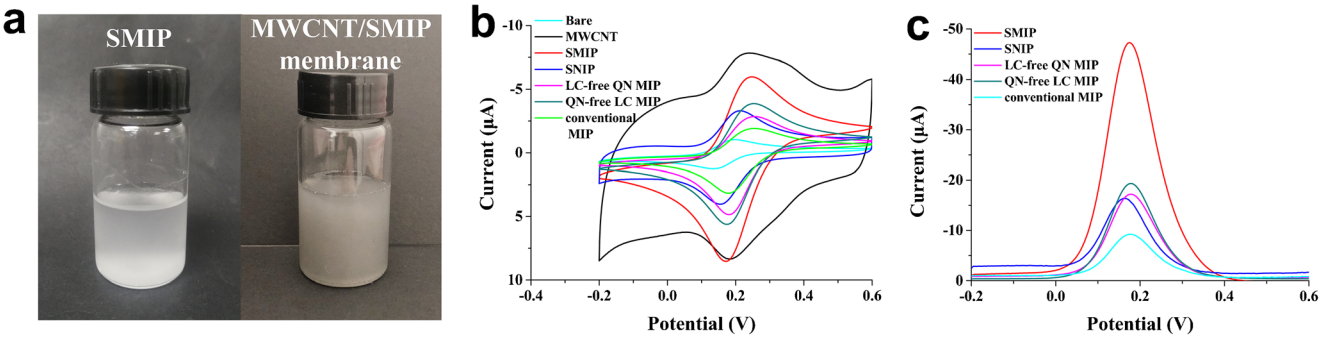

Fig. 8 Dispersion of SMIP and MWCNT/SMIP membrane in acetonitrile/water (5/5, v/v) (**a**) and the CV (**b**) or DPV (**c**) measurements of SMIP, SNIP, and the control composite-modified electrode in the 5 mmol/L $K_3[Fe(CN)_6]$ with 20 mmol/L KCl solution

The Brunauer-Emmett-Teller (BET) surface areas of SMIP and its control composites were further supplied in Table 2. The BET surface area of LC-free QN MIP and conventional MIP with chemical cross-linker (232.68 and 270.49 m^2/g) was over 50 times higher than that of the SMIPs (5.33 m^2/g), which may be related to the non-uniform structure of the high cross-linking that presented as the large surface area that was similar to MWCNT@LC-free MIP we reported previously [5]. Besides, the pure substitution of EDMA with LC monomer and immobile template caused great decrease of total pore volume. Although lower BET surface area and pore volume than that of conventional MIP, the SMIP explicated the higher IF. The results demonstrated that it was the synergistic effect between LC monomer and immobile template rather than surface area improved the imprinting effect of HQN on SMIP.

Electrochemical properties of the SMIP-modified electrode

Figure 8 a has demonstrated SMIP could disperse uniformly in the modified membrane on the MWCNT/SMIP/GCE. Meanwhile, the electrochemical properties of the MWCNT/SMIP-modified electrode (MWCNT/SMIP/GCE) were measured by using the 5 mmol/L $K_3[Fe(CN)_6]$ with 20 mmol/L KCl solution as the electrochemical probe and the CV curves were illustrated in Fig. 8 b. The electrical conductivity of the bare GCE electrode was inferior than that of other GCEs modified by MWCNT, indicating that the MWCNT could enhance the conductivity of the GCE. Since the more imprinted sites accelerated the diffusion of $[Fe(CN)_6]^{3-/4-}$ on the electrode surface, the current intensity of SMIP was far higher. While the MWCNT/conventional MIP was the least, the reason was that the imprinted cavities of the conventional MIP on the electrode surface were embedded with the high level of cross-linker and the electron transfer was hindered. Moreover, the DPV measurements of them were similar to above (Fig. 8c). These results suggested that the LC monomer and immobilized template could improve the electrochemical behavior of the SMIP.

Determination of HQN in lake water

The calibration curve of the HQN in the MWCNT/SMIP/GCE was carried out by DPV responses. As shown in ESM Fig. S4, the reduction peak current increased gradually with the accretion of HQN concentration and had a good linear relationship at the concentration of 0.5–100 μmol/L. The linear equation was $I = -0.594–0.053C$ with the correlation coefficient of 0.997. In accordance with the International Union of Pure and Applied Chemistry (IUPAC) definition, the detection limit (by equation $C_{DL} = 3Sb/m$) is calculated as 0.33 μmol/L. The Sb (0.047) was the standard deviation of the blank ($n = 5$) and m (0.053) was the slope of the linear calibration curve.

In order to confirm its feasibility for real application, the prepared sensor (MWCNT/SMIP/GCE) was used to test the content of HQN in spiked lake water samples. The lake water

Table 3 The determination, recovery and relative standard deviation (RSD) of HQN in lake water samples with the SMIP-based electrochemical sensor ($n = 3$ days, five replicates per day)

Samples	Amount of HQN (μmol/L)		Recovery (%)	RSD (%)	
	Added	Found		Intra-day	Inter-day
Lake water	10	9.74 ± 0.37	97.4	5.5	12.5
	30	29.80 ± 0.63	99.3	2.3	3.2
	50	50.42 ± 0.86	100.8	1.6	3.6

was from the Jingyi lake of Tianjin Medical University and had filtered with the microporous membrane (0.22 μm) before detection. As illustrated in Table 3, the recoveries for the lake water sample analysis varied from 97.4 to 100.8%. The intra-day precision and inter-day precision tests indicated that the RSD values were within 5.5% and 12.5%, respectively. These results proved that the SMIP-based sensor had the promising potential for determination the HQN in complex samples.

Conclusions

In summary, the soluble MIP, stabilized its structure with LC monomer and immobilized template only, was synthesized successfully. Compared with SNIP, QN-free LC MIP, LC-free QN MIP, and conventional MIP, the SMIP exhibited the higher adsorption capacity and imprinted performance for the template (HQN) in acetonitrile/water (5/5, v/v). The selectivity of SMIP on HQN and its analogues QN, HQND and QND, had proved that SMIP could recognize the HQN specifically. Unfortunately, the mechanism on how to stabilize the imprinting site of SMIP in the soluble solvent was not clear yet. The electrode modified by MWCNT/SMIP had presented better conductivity in 5 mmol/L $K_3[Fe(CN)_6]$ solutions. Moreover, the obtained SMIP sensor exhibited highly sensitivity and could detect the trace amount of HQN in lake water. This work provided a good foundation for the preparation of soluble molecularly imprinted polymer.

Funding information This work was supported by National Natural Science Foundation of China (Grant No. 21775109) and Doctoral Startup Foundation of Henan University of Science and Technology (No. 13480055).

Compliance with ethical standards

Conflict of interest The authors declare that they have no conflict of interest.

References

1. Wulff G. Enzyme-like catalysis by molecularly imprinted polymers. Chem Rev. 2002;102:1–27.
2. Wang DD, Gao D, Huang YK, Xu WJ, Xia ZN. Preparation of restricted access molecularly imprinted polymers based fiber for selective solid-phase microextraction of hesperetin and its metabolites in vivo. Talanta. 2019;202:392–401.
3. Song WF, Zhao QL, Zhou XJ, Zhang LS, Huang YP, Liu ZS. A star-shaped molecularly imprinted polymer derived from polyhedral oligomeric silsesquioxanes with improved site accessibility and capacity for enantiomeric separation via capillary electrochromatography. Mikrochim Acta. 2018;186:22.
4. Zhao QL, Zhou J, Zhang LS, Huang YP, Liu ZS. Coatings of molecularly imprinted polymers based on polyhedral oligomeric silsesquioxane for open tubular capillary electrochromatography. Talanta. 2016;152:277–82.
5. Zhang LP, Tan XX, Huang YP, Liu ZS. Floating liquid crystalline molecularly imprinted polymer coated carbon nanotubes for levofloxacin delivery. Eur J Pharm Biopharm. 2018;127:150–8.
6. Zhang LP, Tang SH, Mo CE, Huang YP, Liu ZS. Synergistic effect of liquid crystal and polyhedral oligomeric silsesquioxane to prepare molecularly imprinted polymer for paclitaxel delivery. Eur Polym J. 2018;98:226–36.
7. Usha SP, Gupta BD. Urinary p-cresol diagnosis using nanocomposite of ZnO/MoS2 and molecular imprinted polymer on optical fiber based lossy mode resonance sensor. Biosens Bioelectron. 2018;101:135–45.
8. Saylan Y, Yilmaz F, Özgür E, Derazshamshir A, Yavuz H, Denizli A. Molecular imprinting of macromolecules for sensor applications. Sensors (Basel). 2017;17:898.
9. Liu GY, Huang XD, Li LY, Xu XM, Zhang YG, Lv J, et al. Recent advances and perspectives of molecularly imprinted polymer-based fluorescent sensors in food and environment analysis. Nanomaterials. 2019;9:1030.
10. Li Y, He W, Peng Q, Hou L, He J, Li K. Aggregation-induced emission luminogen based molecularly imprinted ratiometric fluorescence sensor for the detection of Rhodamine 6G in food samples. Food Chem. 2019;287:55–60.
11. Zhang X, Yang S, Jiang R, Sun L, Pang S, Luo A. Fluorescent molecularly imprinted membranes as biosensor for the detection of target protein. Sensor Actuat B-Chem. 2018;254:1078–86.
12. Selvolini G, Marrazza G. MIP-based sensors: promising new tools for cancer biomarker determination. Sensors (Basel). 2017;17:718.
13. Verma A, Murray GM. A path to soluble molecularly imprinted polymers. J Funct Biomater. 2012;3:1–22.
14. Zimmerman SC, Wendland MS, Rakow NA, Zharov I, Suslick KS. Synthetic hosts by monomolecular imprinting insides dendrimers. Nature. 2002;418:399–403.
15. Wulff G, Chong BO, Kolb U. Soluble single-molecule nanogels of controlled structure as a matrix for efficient artificial enzymes. Angew Chem Int Ed Eng. 2006;45:2955–8.
16. Zhang H, Yao RQ, Wang N, Liang R, Qin W. Soluble molecularly imprinted polymer-based potentiometric sensor for determination of bisphenol AF. Anal Chem. 2018;90:657–62.
17. Liang RN, Wang TT, Zhang H, Yao RQ, Qin W. Soluble molecularly imprinted nanorods for homogeneous molecular recognition. Front Chem. 2018;6:81.
18. Palaprat G, Weyland M, Phou T, Binet C, Mauzac M. Introduction of unusual properties into polymers by the use of liquid-crystalline moieties. Polym Int. 2006;55:1191–8.
19. Marty JD, Tizra M, Mauzac M, Rico-Lattes I, Lattes A. New molecular imprinting materials: liquid crystalline networks. Macromolecules. 1999;32:8674–7.
20. Zhang C, Zhang J, Huang YP, Liu ZS. Macromolecular crowding-assisted fabrication of liquid-crystalline imprinted polymers. Anal Bioanal Chem. 2015;407:2923–31.
21. Wei ZH, Mu LN, Huang YP, Liu ZS. Low crosslinking imprinted coatings based on liquid crystal for capillary electrochromatography. J Chromatogr A. 2012;1237:115–21.
22. Liu X, Zong HY, Huang YP, Liu ZS. Liquid crystal-based molecularly imprinted nanoparticles with low crosslinking for capillary electrochromatography. J Chromatogr A. 2013;1309:84–9.
23. Mo CE, Chai MH, Zhang LP, Ran RX, Huang YP, Liu ZS. Floating molecularly imprinted polymers based on liquid crystalline and polyhedral oligomeric silsesquioxanes for capecitabine sustained release. Int J Pharm. 2019;557:293–303.
24. Suriyanarayanan S, Nawaz H, Ndizeye N, Nicholls I. Hierarchical thin film architectures for enhanced sensor performance: liquid crystal-mediated electrochemical synthesis of nanostructured imprinted polymer films for the selective recognition of bupivacaine. Biosensors. 2014;4:90–110.

25. Guerreiro AR, Chianella I, Piletska E, Whitcombe MJ, Piletsky SA. Selection of imprinted nanoparticles by affinity chromatography. Biosens Bioelectron. 2009;24:2740–3.
26. Garcinuño RM, Chianella I, Guerreiro A, Mijangos I, Piletska EV, Whitcombea MJ, et al. The stabilisation of receptor structure in low cross-linked MIPs by an immobilised template. Soft Matter. 2009;5:311–7.
27. Shanks GD. Historical review: problematic malaria prophylaxis with quinine. Am J Trop Med Hyg. 2016;95:269–72.
28. Nontprasert A, Pukrittayakamee S, Kyle DE, Vanijanonta S, White NJ. Antimalarial activity and interactions between quinine, dihydroquinine and 3-hydroxyquinine against Plasmodium falciparum in vitro. Trans R Soc Trop Med Hyg. 1996;90:553–5.
29. Kan HJMV, Jansen PHP, Tuinte C, Smits P, Verbeek ALM. Hydroquinine pharmacokinetics after oral administration in adult patients with muscle cramps. Eur J Clin Pharmacol. 2000;56:263–7.
30. Huston M, Levinson M. Are one or two dangerous? Quinine and quinidine exposure in toddlers. J Emerg Med. 2006;31:395–401.
31. Jansson A, Gustafsson LL, Mirghani RA. High-performance liquid chromatographic method for the determination of quinine and 3-hydroxyquinine in blood samples dried on filter paper. J Chromatogr B Anal Technol Biomed Life Sci. 2003;795:151–6.
32. Mikuš P, Maráková K, Veizerová L, Piešťanský J. Determination of quinine in beverages by online coupling capillary isotachophoresis to capillary zone electrophoresis with UV spectrophotometric detection. J Sep Sci. 2011;34:3392–8.
33. Frosch T, Schmitt M, Popp J. In situ UV resonance Raman microspectroscopic localization of the antimalarial quinine in cinchona bark. J Phys Chem B. 2007;111:4171–7.
34. Holmfred E, Cornett C, Maldonado C, Rønsted N, Hansen SH. An optimised method for routine separation and quantification of major alkaloids in cortex cinchona by HPLC coupled with UV and fluorescence detection. Phytochem Anal. 2017;28:374–80.
35. Tang L, Zhao CY, Wang XH, Li RS, Liu ZS. Macromolecular crowding of molecular imprinting: a facile pathway to produce drug delivery devices for zero-order sustained release. Int J Pharm. 2015;496:822–33.
36. Palisoc ST, Natividad MT, Jesus ND, Carlos J. Highly sensitive AgNP/MWCNT/Nafion modified GCE-based sensor for the determination of heavy metals in organic and non-organic vegetables. Sci Rep. 2018;8:17445.
37. Akhoundian M, Alizadeh T, Ganjali MR, Norouzi P. Ultra-trace detection of methamphetamine in biological samples using FFT-square wave voltammetry and nano-sized imprinted polymer/MWCNTs-modified electrode. Talanta. 2019;200:115–23.
38. Zhang LP, Wang XL, Pang QQ, Huang YP, Tang L, Chen M, et al. Solvent-responsive floating liquid crystalline-molecularly imprinted polymers for gastroretentive controlled drug release system. Int J Pharm. 2017;532:365–73.
39. Zhang LP, Mo CE, Huang YP, Liu ZS. Preparation of liquid crystalline molecularly imprinted polymer coated metal organic framework for capecitabine delivery. Part Part Syst Charact. 2019;36:1800355.
40. Lim KF, Holdsworth CI. Effect of formulation on the binding efficiency and selectivity of precipitation molecularly imprinted polymers. Molecules. 2018;23:2996.
41. Ertürk G, Mattiasson B. Molecular imprinting techniques used for the preparation of biosensors. Sensors (Basel). 2017;17:288.
42. Qian K, Hang G, Wang S. A novel core-shell molecularly imprinted polymer based on metal-organic frameworks as a matrix. Chem Commun. 2011;47:10118–20.
43. Sing KSW. Reporting physisorption data for gas/solid systems with special reference to the determination of surface area and porosity (Recommendations 1984). Pure Appl Chem. 1985;57:603–19.